Eur. Phys. J. Plus (2023) 138:904
https://doi.org/10.1140/epjp/s13360-023-04519-8

THE EUROPEAN PHYSICAL JOURNAL PLUS

Regular Article

Influence of perturbations on linear and nonlinear optical properties of quantum dot

C. O. Edet[1,2,3,a], **E. B. Al**[4,b], **F. Ungan**[4,c], **Etido P. Inyang**[5,d], **N. Ali**[3,6,e], **M. M. Ramli**[7,8,f], **R. Endut**[3,6,g], **S. A. Aljunid**[3,6,h]

[1] Institute of Engineering Mathematics,Universiti Malaysia Perlis, 02600 Arau, Perlis, Malaysia
[2] Department of Physics, Cross River University of Technology, Calabar, Nigeria
[3] Faculty of Electronic Engineering Technology, Universiti Malaysia Perlis, Kangar, Perlis, Malaysia
[4] Physics Department, Faculty of Science, Sivas Cumhuriyet University, 58140 Sivas, Turkey
[5] Department of Physics, National Open University of Nigeria, PMB 581, Jabi-Abuja, Nigeria
[6] Advanced Communication Engineering (ACE) Centre of Excellence Universiti Malaysia Perlis, 01000 Kangar, Perlis, Malaysia
[7] Institute of Nano Electronic Engineering (INEE), Universiti Malaysia Perlis (UniMAP), 01000 Kangar, Perlis, Malaysia
[8] Geopolymer and Green Technology, Centre of Excellence (CEGeoGTech), Universiti Malaysia Perlis (UniMAP), Arau, Perlis, Malaysia

Received: 9 August 2023 / Accepted: 24 September 2023

Abstract This study focused on investigating the influence of perturbations on the linear and nonlinear optical properties of $GaAs/Ga_{1-x}Al_xAs$ screened modified Kratzer potential (SMKP) quantum dot (QD). The optical absorption coefficients (OACs) and refractive index changes (RICs) for $GaAs/Ga_{1-x}Al_xAs$ have been presented. The density matrix and iterative approaches were used to derive expressions of OACs and RICs in SMKP QD. The diagonalization method has been used to obtain energy eigenvalues and eigenfunctions of $GaAs/Ga_{1-x}Al_xAs$ SMKP QD under the effects of Al concentration-x, hydrostatic pressure, and temperature. Our results reveal that the Al concentration-x, hydrostatic pressure, and temperature greatly impact the position and amplitude of the resonant peaks of the linear and nonlinear OACs and RICs. Interpretations have been presented in detail. The results of this study will find applications in the optical physics of semiconductors and other systems.

1 Introduction

Recently, quantum dots (QDs), in which electrons and holes are constrained in all three directions, have drawn much interest for use in optoelectronics and electronic devices [1–3]. Due to recent growth processes, various low-dimensional semiconductor quantum systems can now be produced. In the study and development of light-emitting or detecting devices, quantum-based semiconductors have been widely used [4, 5]. Nonlinear optical properties such as second harmonic generation (SHG) and third harmonic generation (THG), as well as the OACs and RICs, have attracted a lot of interest because they provide in-depth details about the behavior of the structure under the applied structure parameters and the external fields.

Semiconductor nanomaterials are crucial in several fields, such as chip materials and silicon substrate materials in integrated circuits. Because of their excellent flexibility, low power consumption, and great efficiency, contemporary optoelectronic devices and optoelectronic integrated circuits made by combining organic chemicals and semiconductor nanomaterials are very popular. These new innovations in machinery and technology will unavoidably have a significant impact on the traditional industry, which will encourage the modernization of traditional industries [6]. The energy spectrum of the carrier in QDs is discretized because it is entirely constrained, which sharpens the energy state density, and QDs are highly suited for laser applications because of this property [7].

In the literature, a wide range of theoretical studies have been carried out regarding the optical properties of QDs [8–14]. Among these studies, there are many studies investigating the effects of pressure and temperature on OACs and RICs of spherical QDs

[a] e-mail: collinsokonedet@gmail.com
[b] e-mail: emrebahadiral@hotmail.com (corresponding author)
[c] e-mail: fungan@cumhuriyet.edu.tr
[d] e-mail: etidophysics@gmail.com
[e] e-mail: norshamsuri@unimap.edu.my
[f] e-mail: mmahyiddin@unimap.edu.my
[g] e-mail: rosdisham@unimap.edu.my
[h] e-mail: syedalwee@unimap.edu.my

Published online: 10 October 2023

with different potentials [15–22]. In addition, Edet and colleagues studied the effects of confinement potential parameters, optical intensity, magnetic field and the presence of donor impurity on the OACs and RICs in spherical QDs with SMKP [23, 24].

Along with the above review, the distinctive feature of our paper is that it uses the diagonalization method to discuss the nonlinear optical properties of $GaAs/Ga_{1-x}Al_xAs$ QD with SMKP doped with aluminum concentration under the influence of pressure and temperature. Since this research has not been reported yet, we think it has significant practical value for enlarging the varieties of absorbers and enhancing the material's functionality.

The article is organized as follows: Section II describes the methods used to find the energy eigenvalues and eigenfunctions of the system, Part III gives linear and nonlinear OACs and RICs equations, Part IV contains the results obtained and their interpretations, and in Part V, the results obtained are summarized.

2 Model and analysis

Electron in this system is evaluated under the SMKP. Using the effective mass approximation, the Hamiltonian for the electron in $GaAs/Ga_{1-x}Al_xAs$ QD affected by x, P and T has the following form [25]:

$$H = \frac{p^2}{2m^*(x,P,T)} + V(r), \tag{1}$$

where p is the momentum operator of the electron, $m^*(x,\ P,\ T)$ is the effective mass of the electron in the conduction band assumed to depend on x, P and T and it can be expressed as [26]

$$m^*(x,P,T) = \frac{m_0}{1+\frac{28900-6290x}{3}}\left[\frac{2}{E_g^{\Gamma}(x,P,T)} + \frac{1}{E_g^{\Gamma}(x,P,T)+314-66x}\right] + \zeta(x), \tag{2}$$

where m_0 is the mass of free electron, the parameter $\zeta(x) = -3.935+0.488x+4.938x^2$ has an effect on the long-range band effects, $E_g^{\Gamma}(x,\ P,\ T)$ is the energy gap function at the Γ-point, and it can be expressed as:

$$E_g^{\Gamma}(x,P,T) = \lambda_1 + \lambda_2 x + \lambda_3 x^2 + aP - \frac{bT^2}{T_0+T}, \tag{3}$$

where $\lambda_1 = 1519.4\ meV$, $\lambda_2 = 1360\ meV$, $\lambda_3 = 220\ meV$, $a = 107\ meV/GPa$, $b = 0.5405\ meV/K$ and $T_0 = 204\ K$. In Eq. 3, b and T_0 are specific material constants.

$V(r)$ in Eq. (1) is the confinement potential of QD for the charged carrier. To examine the confinement strength and range dependence of QDs, we assume that the structure has the SMKP, i.e., [27]

$$V(r) = D_e\left(q - \frac{r_e}{r}e^{-\alpha r}\right)^2, \tag{4}$$

where $D_e = Q_c\Delta E_g$ is the dissociation energy ($Q_c = 0.6$ is the conduction band offset parameter and $\Delta E_g = 1247x\ (meV)$ [28] is the difference between the band gaps of $Ga_{1-x}Al_xAs$ and $GaAs$ QD materials and depends on the aluminum concentration (x) in $Ga_{1-x}Al_xAs$), r_e is the equilibrium bond length, α is the screening parameter, q is a control parameter whose selection is not random and r is the position of the electron relative to the dot center. The SMKP model is a general case of the modified Kratzer potential obtained for $q = 1$ and $\alpha = 0$, the inverse quadratic Yukawa potential is obtained by setting $q = 0$, and other potential models can be obtained from the SMKP by changing the potential parameters. This type of potential is very important because it contains an attractive Coulombic term and a repulsive inverse square barrier term. The overlapping of these different types of potentials produces a pocket-like potential, and the shape of this potential has great importance for studying the properties of quantum hetero structures.

The time-independent SE can be written as

$$H\psi_{nlm}(r,\theta,\phi) = E_{nlm}\psi_{nlm}(r,\theta,\phi), \tag{5}$$

where n is radial, l is angular momentum and m ($-l \le m \le l$) is azimuthal quantum numbers, ψ_{nlm} and E_{nlm} are three-dimensional eigenfunctions and eigenenergies, respectively. To obtain the energy eigenvalues and eigenfunctions of an electron in a three-dimensional QD under the influence of temperature and pressure, the total Hamiltonian of the system is diagonalized by expanding the complete wave function as [29]

$$\psi_{nlm}(r,\theta,\phi) = \sum_j c_{n_j,l_j}\psi^{(0)}_{n_j l_j m}(r,\theta,\phi), \tag{6}$$

where c_{n_j,l_j} are the expansion coefficients and

$$\psi^{(0)}_{nlm}(r,\theta,\phi) = \varphi^{(0)}_{nl}(r)Y_{lm}(\theta,\phi), \tag{7}$$

is the complete wave function describing the motion of the electron in an infinite spherical QD without the influence of temperature and pressure. The radial part of wave function-$\varphi_{nl}^{(0)}(r)$ is given as

$$\varphi_{nl}^{(0)}(r) = \begin{cases} N j_l(k_{nl} r), & r < R \\ 0, & r \geq R \end{cases}, \tag{8}$$

where R is the radius of the infinite spherical QD and taken as 50 nm, N is the normalization constant and k_{nl} is the nth root of the lth order spherical Bessel function-j_l. Since the spherical harmonics ($Y_{lm}(\theta, \phi)$) are the same for all spherically symmetric potentials, the shape of the potential only affects the radial wave function.

3 Calculation of linear and third-order nonlinear OACs and RICs

The oscillator strength is a very important physical quantity in the study of optical properties related to dipole-allowed absorptions, and it is measurable in photo-luminescence experiments. In addition, the oscillator strength provides additional information about the selection rules of optical absorption. In a dipole-allowed optical transition, the angular momentum values (l) of the respective states must have a difference of ± 1. Therefore, we limit our study to the transition of the ground state ($l = 0$) to the first excited state ($l = 1$). Generally, the oscillator strength-P_{ij} is defined as

$$P_{ij} = \frac{2m^*(x, P, T)}{\hbar^2} E_{ij} |M_{ij}|^2, \tag{9}$$

where $E_{ij} = E_j - E_i$ is the energy difference between two electronic states and $M_{ij} = \langle \psi_i | ez | \psi_j \rangle$ is the electric dipole moment of the transition from state i to state j in QD, where ψ_i and ψ_j are the eigenstates of the system.

To calculate the OACs and RICs of the material due to intersubband transitions, we assume that a polarized monochromatic electromagnetic field interacts with the QD ensemble. The z-polarized electric field vector of this optical wave can be written as

$$\mathbf{E}(t) = (\tilde{E} e^{i\omega t} + \tilde{E}^* e^{-i\omega t}) \hat{z}. \tag{10}$$

where $\tilde{E}$ and ω are the amplitude and frequency of the electromagnetic field, respectively.

Linear, third-order nonlinear and total OACs and RICs for intersubband transitions can be calculated by density matrix approach and perturbation expansion method. In a two-level system approach, we find the following expression for the TOAC [30]:

$$\beta(\omega, I) = \beta^{(1)}(\omega) + \beta^{(3)}(\omega, I), \tag{11}$$

where

$$\beta^{(1)}(\omega) = \sqrt{\frac{\mu}{\varepsilon_r}} \frac{\sigma_s \Gamma_{ij}}{(E_{ij} - \hbar\omega)^2 + (\hbar\Gamma_{ij})^2} \hbar\omega |M_{ij}|^2 \tag{12}$$

and

$$\beta^{(3)}(\omega, I) = -\sqrt{\frac{\mu}{\varepsilon_r}} \left(\frac{I}{2 n_r \varepsilon_0 c} \right) \frac{\sigma_s \Gamma_{ij} \hbar\omega |M_{ij}|^2}{[(E_{ij} - \hbar\omega)^2 + (\hbar\Gamma_{ij})^2]^2} \left[4|M_{ij}|^2 - \frac{\delta_{ij}^2 [3E_{ij}^2 - 4E_{ij}\hbar\omega + \hbar^2(\omega^2 - \Gamma_{ij}^2)]}{E_{ij}^2 + (\hbar\Gamma_{ij})^2} \right] \tag{13}$$

are linear and third-order nonlinear OACs, respectively.

Using the same procedure, the following expression is found for total RICs [31]

$$\frac{\Delta n(\omega, I)}{n_r} = \frac{\Delta n^{(1)}(\omega)}{n_r} + \frac{\Delta n^{(3)}(\omega, I)}{n_r} \tag{14}$$

where

$$\frac{\Delta n^{(1)}(\omega)}{n_r} = \frac{\sigma_s |M_{ij}|^2}{2\varepsilon_r} \frac{E_{ij} - \hbar\omega}{(E_{ij} - \hbar\omega)^2 + (\hbar\Gamma_{ij})^2}, \tag{15}$$

and

$$\frac{\Delta n^{(3)}(\omega, I)}{n_r} = -\frac{\mu c I \sigma_s |M_{ij}|^4}{\varepsilon_r} \frac{E_{ij} - \hbar\omega}{[(E_{ij} - \hbar\omega)^2 + (\hbar\Gamma_{ij})^2]^2} \left[1 - \frac{\delta_{ij}^2 \left[E_{ij}^2 + E_{ij} \left(\hbar\omega + \frac{(\hbar\Gamma_{ij})^2}{E_{ij} - \hbar\omega} \right) - 2(\hbar\Gamma_{ij})^2 \right]}{4|M_{ij}|^2 [(E_{ij} - \hbar\omega)^2 + (\hbar\Gamma_{ij})^2]} \right] \tag{16}$$

are linear and third-order nonlinear RICs, respectively. In the above equations, $\varepsilon_r = n_r^2 \varepsilon_0$ is the real part of the dielectric permittivity, n_r is the refractive index of the semiconductor, ε_0 is the electric permittivity of free space, σ_s is the carrier density, $\delta_{ij} = |M_{jj} - M_{ii}|$, c is the speed of light in free space, μ is the magnetic permeability of the system, $I = 2 n_r c |\tilde{E}|^2$ is the intensity of the electromagnetic field and $\Gamma_{ij} = 1/T_{ij}$ is the intraband relaxation rate, where T_{ij} is the relaxation time.

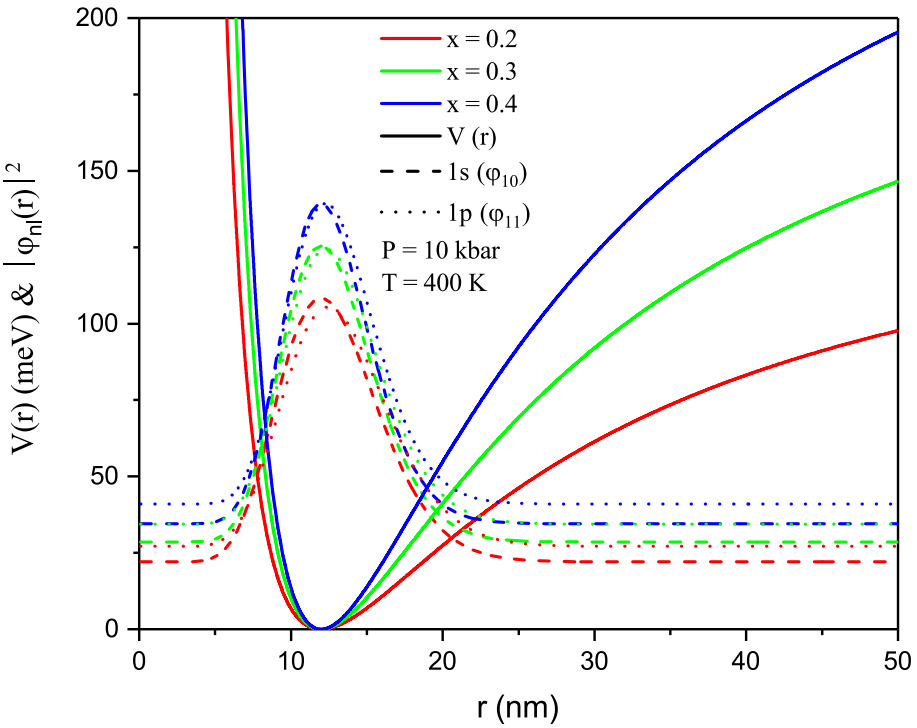

Fig. 1 Plot of confinement potential-$V(r)$ and probability density $|\phi(r)|^2$ as function of r with varying Al concentration-x

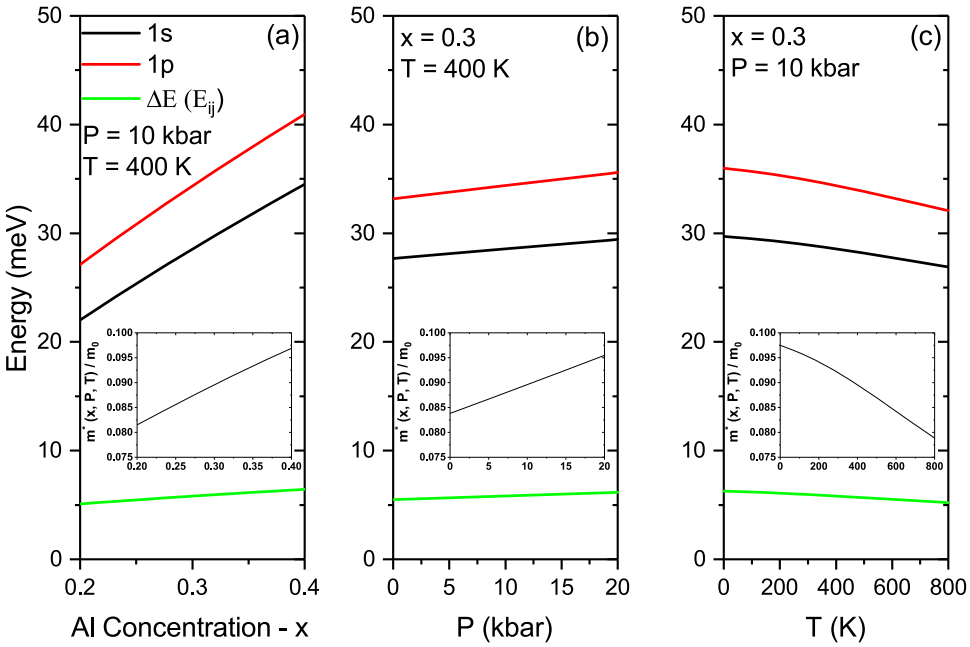

Fig. 2 Plot of Energy (Inset:effective mass of electron in the conduction band) as function of: **a** Al Concentration-x. **b** Pressure (kbar) **c** Temperature for 1 s state (black curve), 1p state (red) and $\Delta E(E_{ij})$ (green curve)

4 Results and discussions

In this section, we have calculated and plotted the OACs and RICs of a spherical *GaAs*/*GaAlAs* QD with SMKP under the influence of pressure and temperature. All calculations were made using the following parameters: $\sigma_s = 1 \times 10^{23}\, m^{-3}$, $T_{ij} = 0.14\, ps$, $n_r = 3.2$, $\mu = 4\pi \times 10^{-7}\, H/m$, $I = 400\, MW/m^2$, $r_e = 1.5$, $q = 1$, $\alpha = 0.05$.

Figure 1 shows the variations in the confinement potential profile of SMKP QD for different *Al* concentration-x. As seen from Fig. 1, as *Al* concentration-x rises, the width of the well becomes narrower, and the well depth increases due to the increase in the dissociation energy. The figure also shows that the amplitude of the wave function peaks increases as the concentration increases, due to the narrowing of the well width. Because the narrower the well, the sharper the localization of the electron.

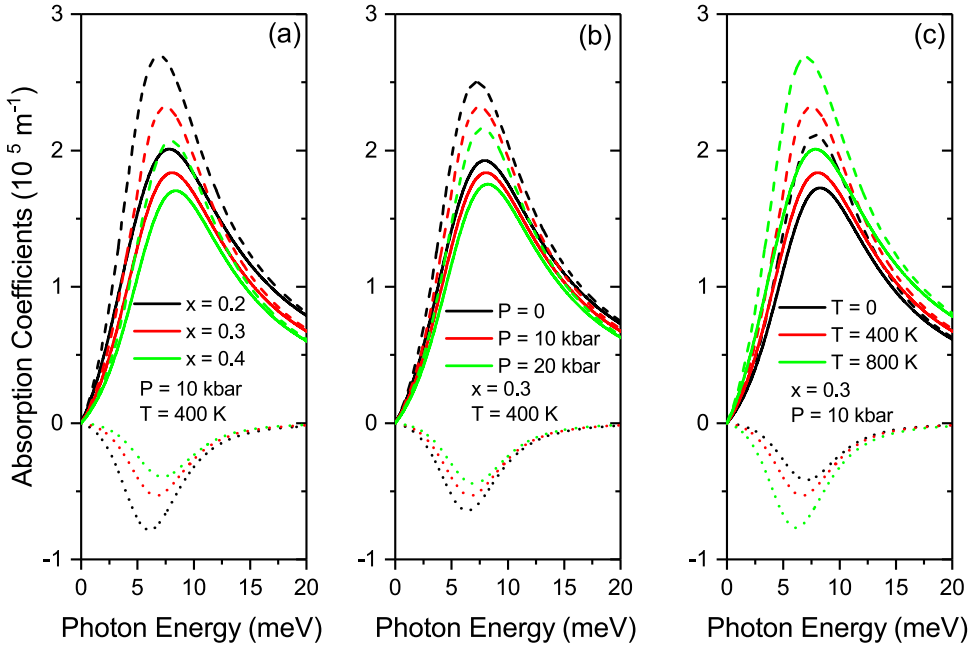

Fig. 3 Plot of *OACs* as function of photon energy with varying **a** Al concentration-x **b** Hydrostatic pressure and **c** Temperature. Dashed lines are for linear, dotted lines are for nonlinear and solid lines are for TOACs

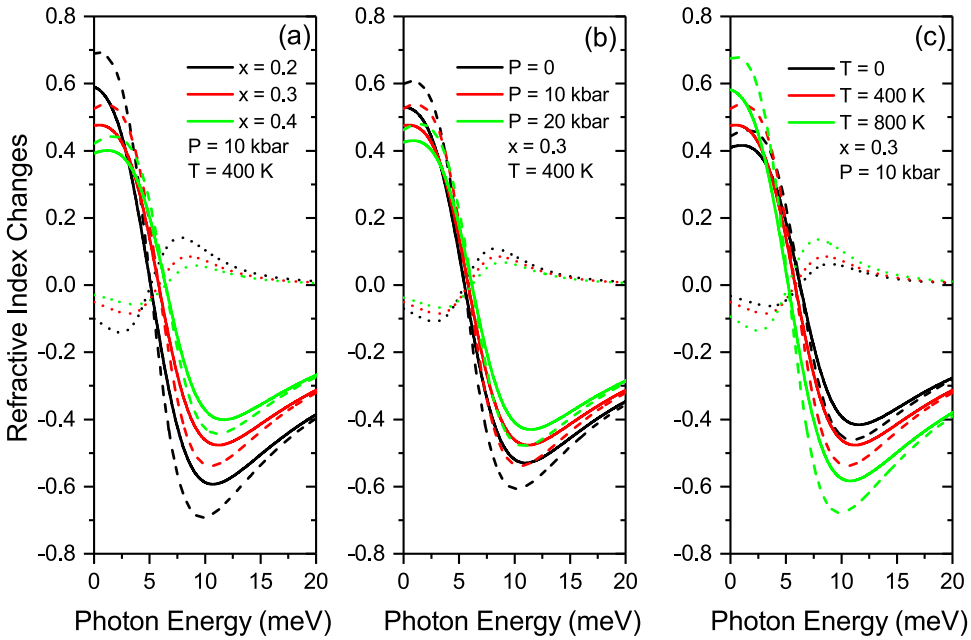

Fig. 4 Plot of *RICs* as function of photon energy with varying **a** Al concentration-x **b** Hydrostatic pressure and **c** Temperature. Dashed lines are for linear, dotted lines are for nonlinear and solid lines are for TOACs

In Fig. 2, we display the energy levels for $1s$, $1p$ and ΔE (difference between the energy levels) versus *Al* concentration-x, pressure (P kbar) and temperature (T K). As seen in Fig. 2a, the $1s$ and $1p$ energy levels increase as the Al concentration increases, due to the narrowing of the well and better localization of the electron. The electron in the $1p$ level senses the narrowing well width with the increase in the Al concentration more than the electron in the $1s$ level, and therefore, the $1p$ energy level increases slightly more than $1s$ as the Al concentration increases. Thus, the energy difference ΔE is also increased. Also, according to Eq. (2), it is seen that the effective mass of the electron in the conduction band $(m^*(x,\ P,\ T)/m_e)$ increases as the Al concentration increases. In Fig. 2b, it is seen that the energies, ΔE and $(m^*(x,\ P,\ T)/m_e)$ tend to increase with the increasing pressure. Because while pressure increases, the effective mass according to Eq. (2) and energy gap function $(E_g^{\Gamma}(x,\ P,\ T))$ at Γ according to Eq. (3) increase. Also, as can be seen from Fig. 2a, there is a parallelism between the change in effective mass and the change in energy. In Fig. 2c, it is seen that the energies, ΔE and $(m^*(x,\ P,\ T)/m_e)$ tend to decrease with the increasing temperature. Because while temperature increases, the effective mass according to Eq. (2) and energy gap function $(E_g^{\Gamma}(x,\ P,\ T))$ at Γ according to Eq. (3) increase. The parallelism between effective mass change and energy change is clearly seen here as well.

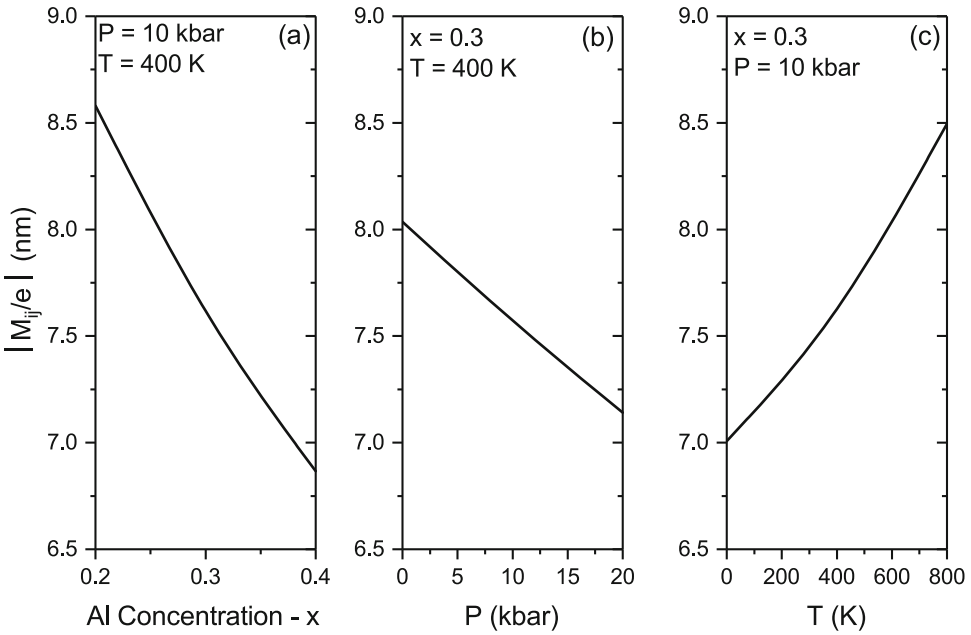

Fig. 5 Plot of *dipole moment matrix elements* as function of **a** Al Concentration-x. **b** Pressure (kbar) **c** Temperature

In Fig. 3, we show the OACs as versus the photon energy for different values of the *Al*-concentration, hydrostatic pressure and temperature. From Fig. 3a, it is shown that the amplitude of the resonant peaks of the linear, third-order nonlinear, and total OACs decrease with rising *Al*-concentration. This behavior is attributed to the fact that as x rises, the quantum confinement effect rises. This characteristic feature agrees with Fig. 1, where we find the changes in the well width plays a major role in the variation in the amplitude of the resonant peaks of the linear, nonlinear and total OACs, and energy difference. It is also seen that when the *Al* concentration increases, the width of the well reduces, the corresponding wave function related with electron spread less and become more localized. However, as can be seen in Fig. 5a, the dipole moment matrix element decreases due to less overlapping of the $1s$ and $1p$ wave functions with the increase in Al concentration, and this directly affects the peak amplitudes of OACs. Also, the peak positions of OACs shift slightly toward higher energy (blue shift) due to the slight increase in ΔE with the increase in Al concentration in Fig. 2a. From Fig. 3b, it is shown that the amplitude of the resonant peaks of the linear, nonlinear and total OACs decrease with rising pressure (P). This behavior is in line with Fig. 2b, which shows that energies and effective mass increase in response to the change in pressure (P). Increasing the energies of the electron in the $1s$ and $1p$ levels causes less overlapping of the wave functions, and as a result, the peak amplitudes of the OACs also decrease with the decrease in the dipole matrix element in Fig. 5b. Similarly, the peak positions of OACs shift slightly to higher energies in parallel with the slight increase in ΔE due to the increase in pressure in Fig. 2b. Figure 3c explicitly shows the effect of temperature on the linear, nonlinear and total OACs. It is shown that the amplitude of the resonant peaks of the linear, nonlinear and total OACs surges with rising temperature T. Because with the increase in temperature, as can be seen in Fig. 2c, the energies and effective mass decrease, and as a result, the dipole matrix element in Fig. 5c increases with more overlapping of the wave functions of the electron at the relevant levels. The position of the resonant peaks shifts toward lower energy (red shift) in relation to the reduction of ΔE as temperature T increases in Fig. 2c. From our results, it is clear that the results in Figs. 2 and 3 agrees fairly. Furthermore, it is explicitly seen that temperature-T has opposite effects with respect to effects of the Al concentration-x and hydrostatic pressure-P on the amplitude and position of the resonant peaks of the linear, nonlinear and total OACs.

In Fig. 4a–c, the linear, third-order nonlinear, and total RICs in a SMKP QD versus of the photon energy are plotted. The parameters used are those specified in the figure. In Fig. 4a, b, we show that magnitude of resonant peaks of the linear, nonlinear and total RICs significantly decreases with rising *Al*-concentration (x) and hydrostatic pressure P. In addition, the blue shift of the resonant peaks with rising *Al*-concentration (x) and hydrostatic pressure P is clearly seen. From Fig. 4c, it is seen that as the temperature-T rises, the amplitude of the resonance peaks of the RICs increases. There is also a red shift due to the decrease in ΔE with temperature in Fig. 2c. These results are in agreement with the variation in OACs (see Fig. 3) and the underlying causes of the changes are the same.

In Fig. 5a–c, we plot the dipole moment matrix elements against the *Al* concentration-x, hydrostatic pressure and temperature. It is clearly shown in Fig. 5a, b that the dipole moment matrix elements decreases with rising *Al* concentration-x and hydrostatic pressure. In Fig. 5c, the dipole moment increases with rising temperature. The increase (decrease) of the dipole moment matrix element with changing parameters is related to more (less) overlapping of electron wave functions at the transition levels.

These properties make our QD a very promising platform for studying nonlinear optical properties of materials.

5 Conclusion

This research article presents the linear, nonlinear and total OACs and RICs in $GaAs/Ga_{1-x}Al_xAs$ SMKP QD influenced by Al concentration-x, hydrostatic pressure (P) and temperature (T). The energy eigenvalues and the energy eigenfunctions are obtained via the diagonalization method. It is seen from our results that amplitude and position of the resonant peaks of the linear and nonlinear OACs and RICs can be manipulated or tuned by these perturbation parameters. By regulating hydrostatic pressure, Al concentration-x and temperature, our numerical further shows that the resonant peaks of the linear and nonlinear OACs and RICs can give rise to a red or blue shift effect. The results obtained in this context can be summarized as follows: (I) Increasing the Al concentration increases the depth of the well and decreases the width of the well, and as a result, the amplitudes of the wave functions and energy levels increase. (II) The increase in Al concentration and pressure increases the examined electron levels, the energy difference between these levels and the effective mass, while it decreases the dipole matrix element. The opposite results are obtained with increasing temperature. (III) Depending on the change in the transition energy and dipole matrix element, with the increase in Al concentration and pressure, the peak positions of OACs and RICs shift to blue, and the peak amplitudes decrease. The effect of temperature is the opposite, both at peak locations and at peak amplitudes. Our results can immensely contribute to experimental and the theoretical investigations of the optical properties of other devices. The significance of these results is that the absorption thresholds lie in the range of low energies (terahertz frequencies). Thus, the frequencies can be controlled by adjusting the Al concentration, pressure and temperature in the $GaAs/Ga_{1-x}Al_xAs$ QD with SMKP. These results can be used in the design of new optoelectronic devices [32–34] for in situ ultrasensitive terahertz spectroscopy [35–38] by the successful deposition of $GaAs/Ga_{1-x}Al_xAs$ QDs specifically on graphene.

Acknowledgements C. O. Edet acknowledges eJDS (ICTP).

Funding COE and NA acknowlegdes the support from the Long-Term Research Grant Scheme (LRGS) Grant LRGS/1/2020/UM/01/5/2 (9012-00009) provided by the Ministry of Higher Education of Malaysia (MOHE). RE and SAA acknowledges the support from the LRGS under Grant Number LRGS/1/2020/UM/01/5/4 (9012-00010) provided by the Ministry of Higher Education Malaysia.

Data Availability Statement This manuscript has associated data in a data repository. [Authors' comment: Data will be made available on reasonable request [37, 38].]

Declarations

Conflict of interest All the authors declared that there is no conflict of interest in this manuscript.

References

1. M. Choubani, D. Makhlouf, F. Saidi, H. Maaref, Enhancement of the second harmonic generation in a coupled lens-shaped quantum dots under wetting layer, temperature, pressure, and electric field effects. Opt. Quant. Electron. **52**, 1 (2020)
2. M. Sayrac, A. Turkoglu, F. Ungan, Influence of hydrostatic pressure, temperature, and terahertz laser field on the electron-related optical responses in an asymmetric double quantum well. Eur. Phys. J. B **94**, 1 (2021)
3. M. Sayrac, Effects of applied external fields on the nonlinear optical rectification, second, and third-harmonic generation in an asymmetrical semi exponential quantum well. Opt. Quant. Electron. **54**, 1 (2022)
4. J. De Jesus, G. Chen, L.C. Hernandez-Mainet, A. Shen, M.C. Tamargo, Strain compensated cdse/znse/zncdmgse quantum wells as building blocks for near to mid-ir intersubband devices. J. Cryst. Growth **425**, 207 (2015)
5. J. Feng, R. Akimoto, S.-I. Gozu, T. Mozume, T. Hasama, H. Ishikawa, Band edge tailoring of ingaas/alassb coupled double quantum wells for a monolithically integrated all-optical switch. Opt. Express **21**, 15840 (2013)
6. M. Karimi, A. Keshavarz, A. Poostforush, Linear and nonlinear intersubband optical absorption and refractive index changes of asymmetric double semi-parabolic quantum wells. Superlattices Microstruct. **49**, 441 (2011)
7. E. Ozturk, Depending on the electric and magnetic field of the linear optical absorption and rectification coefficient in triple quantum well. Opt. Quant. Electron. **49**, 1 (2017)
8. D.A.M. Abo-Kahla, The atomic inversion and the purity of a quantum dot two-level systems. Appl. Math. Inform. Sci. **10**, 1579 (2016)
9. C.M.S. Negi, D. Kumar, J. Kumar, Analysis of polarized light generation in anisotropic strained quantum dots. J. Comput. Electron. **16**, 805 (2017)
10. D. Raeyani, S. Shojaei, S. Ahmadi-Kandjani, Optical graphene quantum dots gas sensors: theoretical study. Superlattices Microstruct. **114**, 321 (2018)
11. K. Zhang, Y.F. Ma, Y.Q. Zhang, H. Gao, Y.B. Han, Concentration modulated photoluminescence and optical switching performance of graphene-oxide quantum dots. J. Lumin. **209**, 116 (2019)
12. A. Naifar, N. Zeiri, S.A.B. Nasrallah, M. Said, Theoretical study on third nonlinear optical susceptibility in inxga1-xn/gan cylindrical quantum dots. Phys. Scr. **95**, 099502 (2020)
13. D.A.M. Abo-Kahla, Information entropy and population inversion of a three-level semiconductor quantum dot. Indian J. Phys. **95**, 1295–1304 (2021)
14. S. Aqiqi, C.A. Duque, A. Radu, J.A. Gil-Corrales, A.L. Morales, J.A. Vinasco, D. Laroze, Optical properties and conductivity of biased gaas quantum dots. Physica E **138**, 115084 (2022)
15. M. Kirak, Y. Altinok, S. Yilmaz, The effects of the hydrostatic pressure and temperature on binding energy and optical properties of a donor impurity in a spherical quantum dot under external electric field. J. Lumin. **136**, 415 (2013)
16. B.A. Farkoush, G. Safarpour, A. Zamani, Linear and nonlinear optical absorption coefficients and refractive index changes of a spherical quantum dot placed at the center of a cylindrical nano-wire: Effects of hydrostatic pressure and temperature. Superlattices Microstruct. **59**, 66 (2013)

17. M.J. Karimi, G. Rezaei, M. Nazari, Linear and nonlinear optical properties of multilayered spherical quantum dots: effects of geometrical size, hydrogenic impurity, hydrostatic pressure and temperature. J. Lumin. **145**, 55 (2014)
18. N. Zamani, A. Keshavarz, H. Nadgaran, Nano multi-layered spherical quantum dot optimization by pso algorithm: Maximizing the optical absorption coefficient. Superlattices Microstruct. **77**, 82 (2015)
19. B. Vaseghi, G. Rezaei, T. Sajadi, Optical properties of parabolic quantum dots with dressed impurity: combined effects of pressure, temperature and laser intensity. Phys. B **456**, 171 (2015)
20. E. Owji, H. Mokhtari, A. Keshavarz, Effects of temperature, pressure, and size on different transitions of optical properties of spherical quantum dot. Iranian J. Sci. Technol. Transact. A **42**, 1669 (2018)
21. N. Aghoutane, M. El-Yadri, A. El Aouami, E. Feddi, F. Dujardin, M. El Haouari, C.A. Duque, C.V. Nguyen, H.V. Phuc, Refractive index changes and optical absorption involving 1s–1p excitonic transitions in quantum dot under pressure and temperature effects. Appl. Phys. A **125**, 17 (2019)
22. N. Aghoutane, L.M. Perez, A. Tiutiunnyk, D. Laroze, S. Baskoutas, F. Dujardin, A. El Fatimy, M. El-Yadri, E.M. Feddi, Adjustment of terahertz properties assigned to the first lowest transition of (d+, x) excitonic complex in a single spherical quantum dot using temperature and pressure. Appl. Sci. **11**, 5969 (2021)
23. C.O. Edet, E.B. Al, F. Ungan, N. Ali, M.M. Ramli, M. Asjad, Effects of the confinement potential parameters and optical intensity on the linear and nonlinear optical properties of spherical quantum dots. Res. Phys. **44**, 106182 (2022)
24. C.O. Edet, E.B. Al, F. Ungan, N. Ali, N. Rusli, S.A. Aljunid, R. Endut, M. Asjad, Effects of applied magnetic field on the optical properties and binding energies spherical gaas quantum dot with donor impurity. Nanomaterials **12**, 2741 (2022)
25. K. Batra, V. Prasad, Spherical quantum dot in kratzer confining potential: study of linear and nonlinear optical absorption coefficients and refractive index changes. Eur. Phys. J. B **91**, 1 (2018)
26. Y. Duan, X. Li, C. Chang, Z. Zhao, L. Zhang, Effects of hydrostatic pressure, temperature and al-concentration on the second-harmonic generation of tuned quantum dot/ring under a perpendicular magnetic field. Physica B **631**, 413644 (2022)
27. C. Edet, A. Ikot, Effects of topological defect on the energy spectra and thermo-magnetic properties of co diatomic molecule. J. Low Temp. Phys. **203**, 84 (2021)
28. S. Adachi, Gaas, alas and $al_x/ga_{1-x}as$: Material parameters for use in research and device applications. J. Appl. Phys. **58**, R1 (1985)
29. E.B. Al, E. Kasapoglu, H. Sari, I. Sökmen, C.A. Duque, Shallow-donor impurity effects on the far infrared electron-electron optical absorption coefficient in single and core/shell spherical quantum dots with konwent-like confinement potential. Opt. Quant. Electron. **54**, 1 (2022)
30. H. Sari, E.B. Al, E. Kasapoglu, S. Sakiroglu, I. Sökmen, M. Toro-Escobar, C. Duque, Electronic and optical properties of a $d_{\mp}^2$ complex in two-dimensional quantum dots with gaussian confinement potential. Eur. Phys. J. Plus **137**, 464 (2022)
31. E.B. Al, Effect of size modulation and donor position on intersubbands refractive index changes of a donor within a spherical core/shell/shell semiconductor quantum dot. Cumhuriyet Sci. J. **42**, 694–701 (2021)
32. H. Cheon, H.-J. Yang, S.-H. Lee, Y.A. Kim, J.-H. Son, Terahertz molecular resonance of cancer dna. Sci. Rep. **6**, 37103 (2016)
33. T. Kampfrath, K. Tanaka, K.A. Nelson, Resonant and nonresonant control over matter and light by intense terahertz transients. Nat. Photon. **7**, 680–690 (2013)
34. K. Sengupta, T. Nagatsuma, D.M. Mittleman, Terahertz integrated electronic and hybrid electronic-photonic systems. Nat. Electron. **1**, 622–635 (2018)
35. A. El Fatimy, R.L. Myers-Ward, A.K. Boyd, K.M. Daniels, D.K. Gaskill, P. Barbara, Epitaxial graphene quantum dots for high-performance terahertz bolometers. Nat. Nanotechnol. **11**, 335–338 (2016)
36. L. St Marie, A. El Fatimy, J. Hruby, I. Nemec, J. Hunt, R. Myers-Ward, D.K. Gaskill, M. Kruskopf, Y. Yang, and R. Elmquist, Nanostructured graphene for nanoscale electron paramagnetic resonance spectroscopy, J. Phys. Mater. **3**, 014013 (2020)
37. A. El Fatimy, A. Nath, B.D. Kong, A.K. Boyd, R.L. Myers-Ward, K.M. Daniels, M.M. Jadidi, T.E. Murphy, D.K. Gaskill, P. Barbara, Ultra-broadband photodetectors based on epitaxial graphene quantum dots. Nanophotonics **7**, 735 (2018)
38. A. El Fatimy, P. Han, N. Quirk, L. StMarie, M.T. Dejarld, R.L. Myers-Ward, K. Daniels, S. Pavunny, D.K. Gaskill, Y. Aytac, T.E. Murphy, P. Barbara, Effect of defect-induced cooling on graphene hot-electron bolometers. Carbon **154**, 497 (2019)